

## **Forsmark site investigation**

### **Mapping of borehole breakouts**

**Processing of acoustical televiewerdata  
from KFM08A, KFM08C, KFM09A,  
KFM09A, KFM09B and KFM90B**

Jørgen Ringgaard, Rambøll A/S

June 2007

**Svensk Kärnbränslehantering AB**

Swedish Nuclear Fuel  
and Waste Management Co  
Box 5864

SE-102 40 Stockholm Sweden

Tel 08-459 84 00

+46 8 459 84 00

Fax 08-661 57 19

+46 8 661 57 19



## **Forsmark site investigation**

### **Mapping of borehole breakouts**

#### **Processing of acoustical televiewerdata from KFM08A, KFM08C, KFM09A, KFM09A, KFM09B and KFM90B**

Jørgen Ringgaard, Rambøll A/S

June 2007

*Keywords:* AP PF 400-06-119, Borehole breakouts, Televiewer, Deformations, Micro fallouts.

This report concerns a study which was conducted for SKB. The conclusions and viewpoints presented in the report are those of the author and do not necessarily coincide with those of the client.

Data in SKB's database can be changed for different reasons. Minor changes in SKB's database will not necessarily result in a revised report. Data revisions may also be presented as supplements, available at [www.skb.se](http://www.skb.se).

A pdf version of this document can be downloaded from [www.skb.se](http://www.skb.se).

# Abstract

This report presents a detection and mapping of borehole breakouts and other borehole deformations by means of processing of data from an acoustical televiewer probe. Special attention is paid to small breakouts and micro fallouts.

The registration is done in Excel-sheets in a table and a chart, which show the main azimuth of the breakouts. The charts show an obvious tendency, that the main azimuth of the breakouts and micro fallouts is found to be at 40 to 80° from magnetic north.

Due to the inclination of the boreholes, the televiewer is slightly decentralized during logging, which causes reduced data quality. But despite this, breakouts, keyseats and washouts with a certain magnitude (more than 0.1 mm), can still be mapped and classified after centralization of data by special processing routines.

Also micro fallouts (fallouts smaller than 0.1 mm) can be registered, but the mapping of these is more uncertain, as is it not possible to make specific criteria for this phenomenon. The detection has been done as a visual inspection and it is often hard to determine the area of distribution of these small structures. In some cases the micro fallouts are found to be in the entire perimeter of the borehole, but in other cases they have a main azimuth in the same direction as the breakouts.

In one of the investigated boreholes, KFM08A, two televiewer surveys were performed with a time difference of about two years. This enabled a study of the time dependence of borehole breakouts and other deformation processes in this borehole. However, any deformation differences between the two measurement occasions were not revealed.

# Sammanfattning

Denna rapport redovisar förekomsten och kartering av borrhålsspjälkning och andra borrhålsdeformationer, baserat på data från en akustisk televiwersond. Särskild vikt har lagts vid mycket små borrhålsspjälkningar och mikroutfall.

Dataregistreringen är utförd i Excel-blad i tabeller och diagram, vilka illustrerar huvud-azimuth för spjälkningarna. Diagrammen visar en tydlig tendens, att huvudazimuth för spjälkning och mikroutfall finns i intervallet 40–80° från magnetisk norr.

Pga borrhålens lutning är televiwersonden svagt decentraliserad under loggningen, vilket leder till sämre datakvalité. Trots detta är det möjligt att urskilja spjälkning, keaseats och washouts med bestämd magnitud (mer än 0,1 mm). Detta kan åstadkommas genom att centralisering kan göras genom en speciell dataprocessrutin.

Även mikro utfall (utfall mindre än 0,1 mm) kan urskiljas, men karteringen av dessa är mer osäker, då det inte är möjligt att precisera kriterium för detta. Identifiering har kunnat göras genom visuell bedömning men ofta är det svårt att avgöra utbredningen av mikroutfallen. I några fall har mikroutfall förekommit i hela borrhålets perimeter, men i andra fall har de haft huvudazimuth i samma riktning som spjälkningen.

Ett av borrhålen, KFM08A, har loggats två gånger med televiwersonden, med ca två års tidskillnad. Detta har möjliggjort en studie av borrhålsspjälkningens övriga deformationsprocessers tidsberoende i detta borrhål. Några deformationsskillnader mellan de två loggningstillfällena kunde dock inte påvisas.

# Innehåll

<b>1</b>	<b>Introduction</b>	7
<b>2</b>	<b>Objective and scope</b>	11
<b>3</b>	<b>Equipment</b>	13
<b>4</b>	<b>Processing of data</b>	15
4.1	Import and orientation	15
4.2	Alignment of images	15
4.3	Filtering and calculation of decentralization	17
4.4	Centralization of images	17
4.5	Calculation of calipers and ovality	17
4.6	Registration of breakouts and other deformations	18
4.7	Nonconformities	18
<b>5</b>	<b>Description of logpanel</b>	19
5.1	Explanation of logs	19
5.1.1	Amplitude	19
5.1.2	Caliper max position	19
5.1.3	Caliper min position	19
5.1.4	Caliper – max – Centralized – Median filtered	19
5.1.5	Caliper – mean – Centralized – Median filtered	19
5.1.6	Caliper – min – Centralized – Median filtered	19
5.1.7	Class	19
5.1.8	Cross-section – Radius – Centralized	20
5.1.9	Decentralization	20
5.1.10	Radius – Centralized	20
5.1.11	Radius – Centralized – Median filtered	20
5.1.12	Radius – Centralized – Median filtered – median	20
5.1.13	Radius – Median filtered – max	20
5.1.14	Radius – Median filtered – median	20
5.1.15	Radius – Median filtered – mean	20
5.1.16	Radius – Median filtered – min	20
5.1.17	Tool rotation	20
<b>6</b>	<b>Analysis and registration of observed deformations</b>	21
6.1	Classification of observed deformations	21
6.2	Explanation of columns in the excel-sheet	21
6.3	Examples of borehole deformations	22
6.3.1	Example of borehole breakout (BB)	22
6.3.2	Example of washout (WO)	22
6.3.3	Example of keyseat (KS)	24
6.3.4	Example of micro fallout (MF)	24
6.4	Explanation of special features in the boreholes	25
6.4.1	Tracks from decentralization	25
6.4.2	Drill cuttings from bottom of borehole	26
6.4.3	Wobbles from drilling process	26
6.5	Specific features in the boreholes	26
6.5.1	KFM08A. April 2005	26
6.5.2	KFM09A	26
<b>7</b>	<b>Time dependence of breakout</b>	29
<b>8</b>	<b>Summary and discussions</b>	31

**Appendices on CD**

**Appendix A** List of acquisition reports

**Appendix B** Tables and charts of depth errors

KFM08A

KFM08C

KFM09A

KFM09B

**Appendix C** Tables and charts of registered deformations

KFM08A. April 2005

KFM08A. March 2007

KFM08C

KFM09A

KFM09B

KFM90B

**Appendix D** Plot of logpanels

Appendix D KFM08A\_Breakout\_April\_2005

Appendix D KFM08A\_Breakout\_March\_2007

Appendix D KFM08C\_Breakout

Appendix D KFM09A\_Breakout

Appendix D KFM09B\_Breakout

Appendix D KFM90B\_Breakout

# 1 Introduction

Boreholes and tunnels in sedimentary formations as well as in bedrock may, during certain conditions governed by the relation between the compressive strength of the rock material and the state of stress, be exposed to spalling, often referred to as borehole breakouts, entailing that the originally circular borehole perimeter is deformed and changes its geometry to a more or less oval shape. (More exact definitions and a classification of borehole deformations of different types are given in Section 6.1.) The orientation of breakouts is governed by the stress field, such that the breakouts (ideally) occur on opposite sides of the borehole in the same bearing as that of the minor horizontal stress.

Width, length and depth of breakouts may vary within broad ranges, reflecting variations in the rock strength-/rock stress relation /Zoback et al. 1985/ and possibly also mirroring the impact of the drilling process /Ask et al. 2006/. The study of breakouts is primarily aiming at shedding light on the orientation of the stress field and its continuity. Secondly, breakouts may be used also for determination of stress magnitudes, however mainly as a supporting method.

It has previously been shown that spalling phenomena may well be identified and characterized by the analysis of acoustic televiewer images e.g. /Deltombe and Schepers 2000, Siddans and Worthington 2003/. Due to the high accuracy of the acoustic televiewer method for determination of geometrical properties of the borehole, it is especially advantageous when addressing minor deformations, which may be very difficult to detect with other methods.

A pilot study aiming at investigating the potential of the acoustic televiewer method of identifying and characterizing major as well as minor borehole deformations in the rock types prevailing at Forsmark was performed during 2005 /Ask and Ask 2006, Ask et al. 2006/. Two subvertical core drilled boreholes, KFM01A (1,000 m long) and KFM01B (500 m) were investigated. The applicability of the method was clearly demonstrated and a range of borehole deformations of different dimensions was revealed in both boreholes.

This pilot study was followed by a more extensive study in 2006 of borehole breakouts and other deformation processes from results of televiewer loggings in the Forsmark boreholes KFM01A, KFM01B, KFM02A, KFM03A, KFM03B, KFM04A, KFM05A, KFM06A and KFM07C /Ringgaard 2006/. The successful results from that study implied the continued study of deformation processes presented in this report.

According to the theory for the generation of borehole breakouts, some degree of time dependence may be inherent in the process. In other words, the areal extension and amplitude of breakouts as well as their frequency in a specific borehole may, theoretically, increase versus the elapsed time after completion of drilling, until the stress field around the borehole has stabilized and steady-state conditions have been obtained. The degree of time dependence is due to several factors. In order to study this effect, two acoustical televiewer loggings with a time span of approximately two years have been performed in borehole KFM08A. By analysis of the results of the two surveys, conclusions is drawn whether the breakout generating process has been active between drilling completion and the first televiewer logging in April 2005 respectively between the first televiewer logging and the second televiewer logging in March 2007.

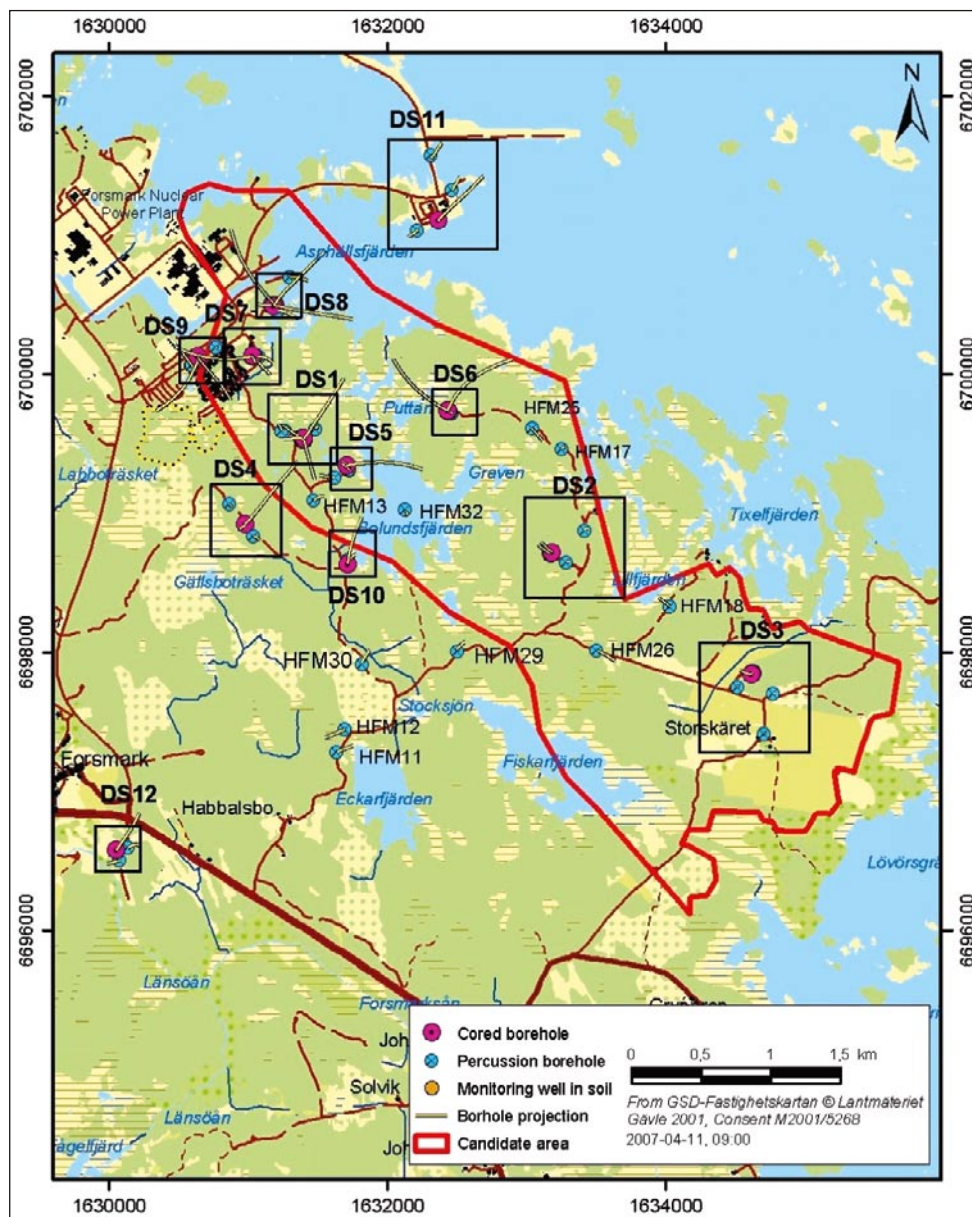
This document reports the results gained by processing and interpretation of acoustic televiewer data from five boreholes at Forsmark, which is one of the activities performed within the site investigation at Forsmark. The work was carried out in accordance with Activity Plan AP PF 400-06-119, see Table 1-1. Activity Plans and Method Descriptions are SKB's internal controlling documents. However, for the activity presented in this report, there exists no SKB Method Description.

A map of the Forsmark investigation area is presented in Figure 1-1, whereas details of the different drill sites are shown in Figure 1-2.

Original data from the reported activity are stored in the primary database Sicada. Data are traceable in Sicada by the Activity Plan number (AP PF 400-06-119). Only data in databases are accepted for further interpretation and modelling. The data presented in this report are regarded as copies of the original data. Data in the databases may be revised, if needed. Such revisions will not necessarily result in a revision of the P-report, although the normal procedure is that major revisions entail a revision of the P-report. Minor revisions are normally presented as supplements, available at [www.skb.se](http://www.skb.se).

**Table 1-1. Controlling document for performance of the activity.**

Activity plan	Number	Version
Detection of potential borehole breakouts in boreholes KFM08A, KFM08C, KFM09A, KFM09B and KFM90B	AP PF 400-06-119	1.0



*Figure 1-1. Map of borehole locations at the Forsmark investigation area.*



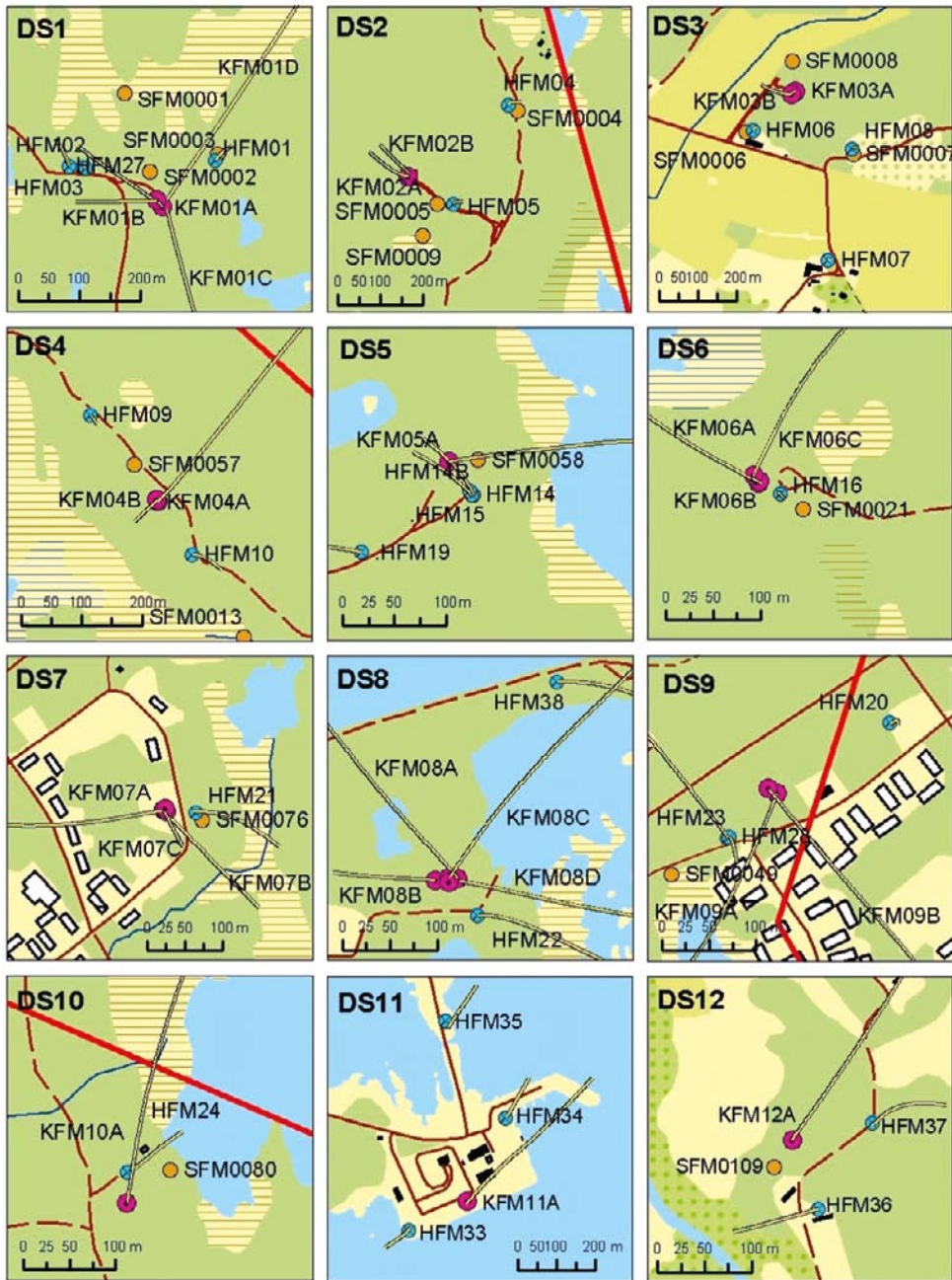


Figure 1-2. Detailed maps of the different drill sites.

## 2 Objective and scope

Efforts to map the effects of the stress in the Forsmark region have been done with a suite of methods. This report describes a special processing of televiewer data with attention to the effect of stress: deformations of the borehole. The mapping is done according to the SKB-document AP PF 400-06-119. An overview of the processed boreholes can be found in Table 2-1.

**Table 2-1. Overview of boreholes (from Sicada).**

Borehole	Length [m]	Inclination [° from hor.]	Orientation [° from GN]
KFM08A	1,001.0	-60.11	319.42
KFM08C	951.1	-60.46	35.88
KFM09A	799.7	-59.90	200.10
KFM09B	616.5	-55.08	140.83
KFM90B	18.2	-82	262

### 3 Equipment

The probe used for acquisition of data is a High Resolution Acoustical Televiwer (HiRAT) from Robertson Geologging Ltd. <http://www.geologging.com/>.

The transducer is a 1.5 MHz head, which transmits the acoustic signal via a rotating acoustic mirror to the borehole wall. The strength of the reflected signal is recorded as an Amplitude log, while the first arrivals are picked and stored in a Traveltime log. Both logs are stored as images with selectable horizontal resolution from 90 to 360 pixels/revolution and a vertical resolution depending on the logging speed. The radial resolution in the recorded Traveltime is 100 nS, which equals 0.075 mm. The boreholes were logged with different selections of resolution; an overview of this is shown in Table 3-1.

The images are oriented by means of a built-in orientation unit containing a 3-axis fluxgate magnetometer as well a 3-axis accelerometer. The output from this device can also be used to calculate a deviation log for the borehole.

The probe is centralized in the borehole with two bow spring centralizers; see the picture in Figure 3-1. The applied centralizers are designated to boreholes with diameters in the range 67–100 mm.

For detailed information regarding the data acquisition with the HiRAT probe, please refer to SKB reports listed in Appendix A.

**Table 3-1. Overview of resolutions.**

Borehole	Pixels/rev.	Horisontal res. [mm]	Logging speed [m/min.]	Vertical res. [mm]
KFM08A_2005	90	2.7	10	8
KFM08A_2007	120	2.0	2.3	2
KFM08C	180	1.3	2.3	2
KFM09A	90	2.7	10	8
KFM09B	90	2.7	10	8
KFM90B	180	1.3	2.3	2



*Figure 3-1. Picture of HiRAT probe.*

## 4 Processing of data

The final processing of the televiewer-data contains the steps described below. A lot of effort has been spent to investigate different possibilities in the processing. Only the final processing done to the delivered data is described. All processing is done in WellCAD, which is made by Advanced Logic Technology. A free reader for WellCAD documents can be downloaded on [www.alt.lu](http://www.alt.lu).

### 4.1 Import and orientation

The televiewer data are recorded in the dedicated logging-program HiRAT from Robertson Geologging Ltd. The data are stored in time domain, with a table which links the data to depth.

Image-data as well as orientation-data are imported and resampled to depth-domain. Orientation-data are filtered with a 25 samples moving average filter. Images are resampled to 360 pixels/rev. before orientation. This is done to prevent fractures from being edged during orientation.

Images are then oriented to Magnetic North (MN) by means of data from the orientation unit.

### 4.2 Alignment of images

In order to provide a system for length calibration of different logging systems used at the site investigation, reference tracks (grooves) have been milled into the borehole wall with a specially designed tool at regular levels in all cored drilled boreholes. Regarding televiewer logging, the length calibration is conducted as follows.

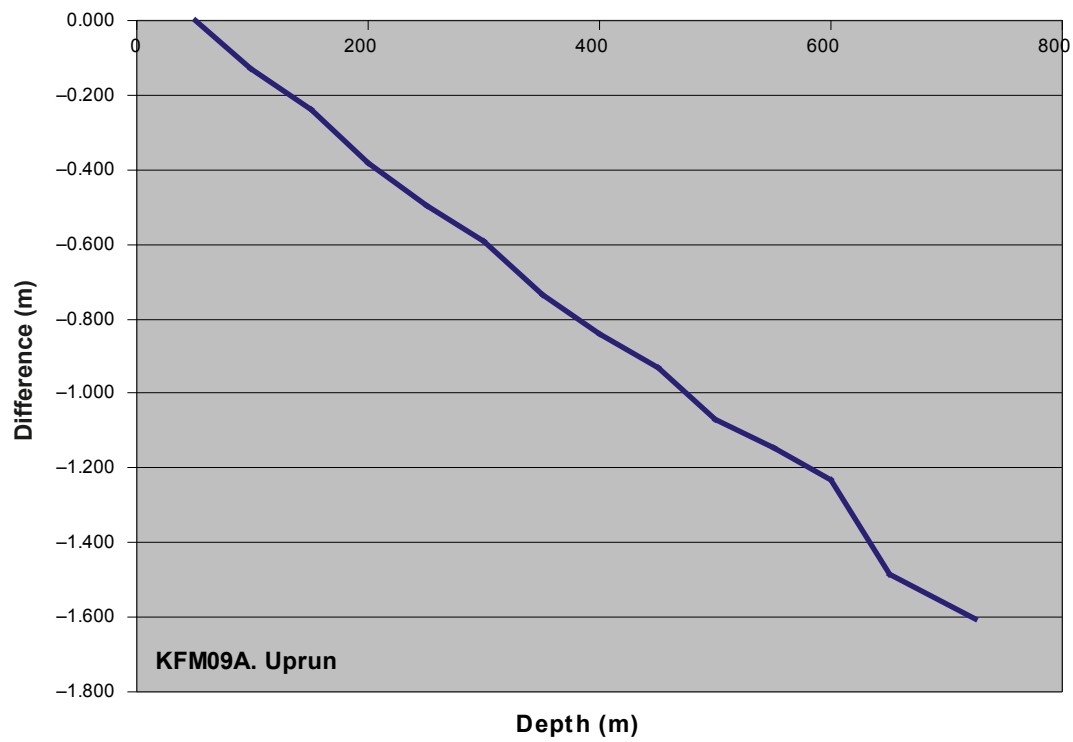
First all HiRAT logs are shifted, so that the upper edge of the top-most track is aligned to the milled reference track. Then all tracks in the borehole are identified and a table is made. An example of this is shown in Table 4-1.

Also a plot of the differences is made. This is done to check the linearity of the depth error. An example of a plot is shown in Figure 4-1. The depth tables and plots of all boreholes can be found in Appendix B.

All logs are then stretched to fit the milled tracks in the borehole, which results in a perfect alignment to the tracks.

**Table 4-1. Example of depth table. KFM09A.**

True depth [m]	HiRAT [m]	Difference [m]
50.000	50.000	0.000
99.000	99.127	-0.127
150.000	150.239	-0.239
200.000	200.380	-0.380
250.000	250.498	-0.498
300.000	300.594	-0.594
350.000	350.737	-0.737
400.000	400.841	-0.841
450.000	450.930	-0.930
500.000	501.069	-1.069
550.000	551.146	-1.146
600.000	601.234	-1.234
650.000	651.486	-1.486
725.000	726.602	-1.602



*Figure 4-1. Example of plot of depth error. KFM09A.*

### 4.3 Filtering and calculation of decentralization

To calculate the decentralization, the Traveltime image needs to be filtered with a 15×15 pixels weighted average filter, which equals an area of 30×30 mm with 2×2 mm pixelsize. In boreholes with lower resolutions, the filter-size is reduced proportionally. This is done to prevent small fractures from disturbing the decentralization calculation. Then the image is converted from Traveltime (the unit is 100 nS) to radius with the formula:

$$Radius(mm) = \frac{(Travel\ Time - Internal\ Traveltime \times 10) \times VEL(FL)}{10 \times 1000} + tool\ radius$$

where “VEL(FL)” is the sound velocity in the borehole fluid

“Internal Traveltime” is the internal traveltime in the oil from the transducer to the acoustic window of the HiRAT tool. As the sound velocity in the oil has a small temperature coefficient, it is calculated as:

$$Internal\ Traveltime = \frac{(-2.24 \times TEMP(FL) + 1031) \times 120}{1000}$$

“TEMP(FL)” is the temperature of the water in the borehole, which was measured with a 9042 FluidRes and FluidTemp probe from Century Geophysical (see overview of acquisition reports in Appendix A). Also VEL(FL) is calculated in the reports, from the measured resistivity of the fluid.

Next step is to extract statistics from the new radius image log, which returns logs for minimum, maximum, average and median values of the radius image. From these the decentralization of the probe is calculated as:

$$Decentralization = "Radius - mean" - "Radius - min"$$

### 4.4 Centralization of images

Due to the inclination of the boreholes, the acoustic televiewer-probe is slightly decentralized during logging; the size of this decentralization is roughly 0.1 mm/deg. from vertical. Therefore a centralization routine is applied to compensate the images for this. This is done by means of a sine-fitting routine in WellCAD. It can be done only to the Traveltime (Radius) image, not to the Amplitude image.

### 4.5 Calculation of calipers and ovality

The Centralized Traveltime is then also converted to a radius image as described in 4.3 and the previous image is deleted.

Now mean, minimum and maximum calipers as well as angles (eg. Caliper Max Position) for these can be extracted from the median filtered image log. Then the extracted angles (position logs) are filtered again with a 100 pts. (2 metres) moving average filter; this is done to smoothen the logs as only main angles are of interest.

An ovality log can now be calculated as twice the median radius minus the minimum caliper.

$$OVALITY - MIN = "Radius - Centralized - Median filtered - median" \times 2 - "Caliper - min - Centralized - Median filtered"$$

This ovality log will only be reliable where some ovality is present, as it will be smeared by the fractures in the borehole as well as method introduced artefacts. It also needs to be compared with the angle logs, which should be stable in one direction, before an eventual ovality can be considered reliable.



As a manual check of the ovality, cross-section logs are generated every 20 metres, as well as right above and below breakouts (the latter are deleted again). These cross-sections have grid-circles every 0.5 mm, allowing the ovality to be visually checked, see example in Figure 4-2 below.

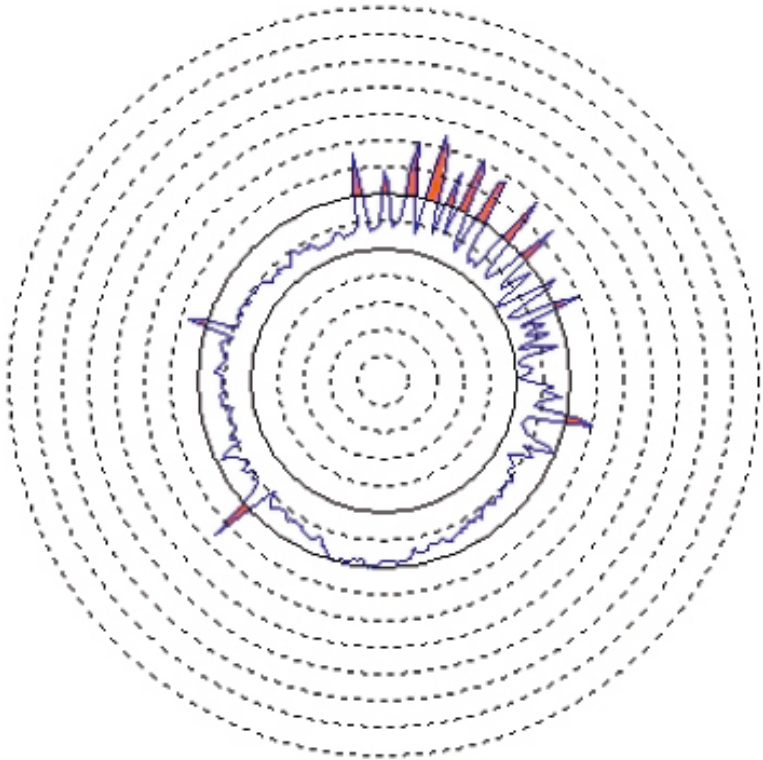
When necessary, the same process is applied to the downrun and imported to the uprun log-panel. It is used in case of doubt to help separating real deformations from artefacts. The Radius image is deleted again.

### 4.6 Registration of breakouts and other deformations

To register and describe deformations, the log panel is manually inspected. When necessary a cross-section is generated and the deformation is classified, measured and registered in an Excel-table. In Figure 4-2 below is shown an example of a cross-section. The spacing between the radial grid here is 0.1 mm. The spikes on the cross-section, which have a maximum size of 0.3 mm, show some roughness on the borehole wall – micro fallout.

### 4.7 Nonconformities

The activity was performed in compliance with Activity Plan AP PF 400-06-119 without deviations.



*Figure 4-2. Example of cross-section with micro fallout.*



## 5 Description of logpanel

### 5.1 Explanation of logs

Here follows – in alphabetic order – a description of all the logs in the panel.

#### 5.1.1 Amplitude

Amplitude of the returned acoustic signal from the borehole wall. Darker (more blue) colours represent low amplitude – softer surface, while lighter (more yellow) colours represent high amplitude – harder surface of wall. The log is (as all other images) shown as an un-rolled 360° image of the borehole, where 0° is the reference, which is aligned against magnetic north (MN). The image has no unit.

#### 5.1.2 Caliper max position

Orientation of the calculated maximum caliper in degrees from MN of the borehole. The log is derived from the filtered and centralized radius image. Contains values from 0–180 degrees.

#### 5.1.3 Caliper min position

Orientation of the calculated minimum caliper in degrees from MN of the borehole. The log is derived from the filtered and centralized radius image. Contains values from 0–180 degrees.

#### 5.1.4 Caliper – max – Centralized – Median filtered

Maximum caliper measured in the median filtered and centralized radius image. Unit: mm.

#### 5.1.5 Caliper – mean – Centralized – Median filtered


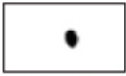

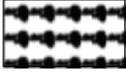
Mean caliper measured in the median filtered and centralized radius image. Unit: mm.

#### 5.1.6 Caliper – min – Centralized – Median filtered

Minimum caliper measured in the median filtered and centralized radius image. Unit: mm.

#### 5.1.7 Class

Symbol log, which shows the classification of registered deformations. This log is pasted from the column in the registration Excel-sheet.

BB		Borehole Breakout
KS		Key Seat
MF		Micro Fallout
WO		Washout

### **5.1.8 Cross-section – Radius – Centralized**

Cross-sections are generated every 20 metres in the borehole. The cross-section is averaged over 10 cm. Radii below the actual nominal radius are shaded green, and radii above are shaded orange.

### **5.1.9 Decentralization**

Calculated decentralization as the difference between the mean and min radius of the radius image. Unit: mm.

### **5.1.10 Radius – Centralized**

Radius image log, which is centralized as described to compensate for decentralization of the probe. Light colours represent smaller radii, while darker colours represent larger radii. Unit: mm.

### **5.1.11 Radius – Centralized – Median filtered**

Radius image log, which is centralized as described earlier and median filtered over an area of 15×15 pixels (app. 20×30 mm) to shade for small deformations, when calculating calipers. Light colours represent smaller radii, while darker colours represent larger radii. Unit: mm.

### **5.1.12 Radius – Centralized – Median filtered – median**

This log is not shown; it is used to calculate the ovality as described in Paragraph 4.5.

### **5.1.13 Radius – Median filtered – max**

Maximum radius of the median filtered, but not centralized radius image, unit: mm.

### **5.1.14 Radius – Median filtered – median**

Median radius of the median filtered, but not centralized radius image, unit: mm.

### **5.1.15 Radius – Median filtered – mean**

Mean radius of the median filtered, but not centralized radius image, unit: mm.

### **5.1.16 Radius – Median filtered – min**

Minimum radius of the median filtered, but not centralized radius image, unit: mm.

### **5.1.17 Tool rotation**

Shows the rotation of the probe, as the borehole was logged, unit: degrees.

## 6 Analysis and registration of observed deformations

### 6.1 Classification of observed deformations

In Appendix C tables with classification of all interpreted deformations in the boreholes are found. The classification is illustrated in Figure 6-1.

### 6.2 Explanation of columns in the excel-sheet

The columns in the Excel-sheet are explained as follows:

**Top Depth:** Top of the deformation.

**Bot. Depth:** Bottom of the deformation.

**Max. R:** Maximum radius of the deformation, read from “Radius – max – Median Filtered”-log and/or “Radius” image.

**Median R:** Nominal radius at the depth, read from “Radius – median – Median Filtered”-log.

**dRmax:** Delta radius, i.e. the depth of the deformation into the borehole wall.

**Structure:** Classification of the deformation. Examples and further explanation are shown in Paragraph 6.3.

BB: Borehole breakout

WO: Washout

KS: Key seat

MF: Micro fallout

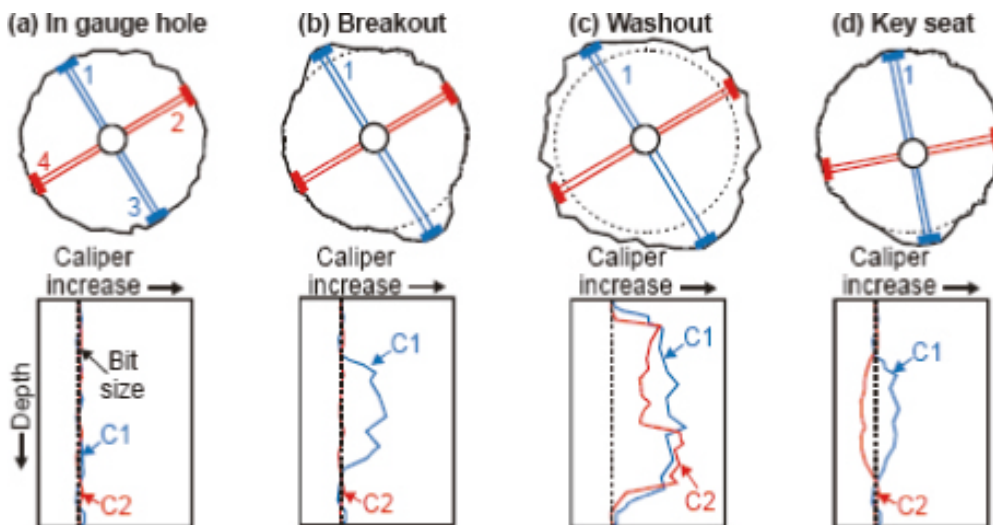
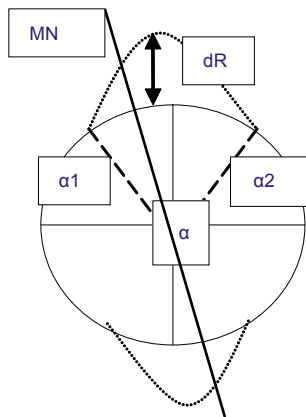


Figure 6-1. Classification of deformations from /Ask and Ask 2006/ after /Plumb and Hickman 1985/.



**Figure 6-2.** Illustration of angles.

**Uncertainty:** The uncertainty of the observed deformation: 3 = certain, 2 = probable, 1 = possible, 0 = not estimated. The uncertainty is primary related to the type of deformation.

**Cross. struct.:** The deformation is related to a fracture crossing the borehole. Example of this is shown in Paragraph 6.3.

**Main azimuth:** Main azimuth of the deformation in degrees from Magnetic North. The angle is calculated from the next column “Azimuth”. If the angle is between 0 and 180°, the main azimuth is the same, but if the azimuth is between 180 and 360°, 180° are subtracted from the angle. Example of this is shown and explained in Paragraph 6.3.

**Azimuth:** Angle from MN to the dominating point of the deformation.

**Aperture $\alpha$ 1:** Angle from MN to first edge of the deformation. If the deformation is located around 0° MN, this angle is noted as a negative angle from MN, e.g. -5°. This angle equals 355°.

**Aperture $\alpha$ 2:** Angle from MN to last edge of the deformation.

## 6.3 Examples of borehole deformations

### 6.3.1 Example of borehole breakout (BB)

In Figure 6-3 an example of borehole breakout from KFM07C is shown. As there are obvious diametrically opposite deep fallouts, this deformation is Classified as BB with the uncertainty as “3” – most certain. As the breakout is seen to be in connection with a fracture crossing the borehole, a “Y” (Yes) is placed in the “Crossing structure” column. Here the deepest and most dominating fallout is seen at 50° and the aperture of the fallout is read to be from 0 to 100°.

The centralization routine is only perfect in a truly circular borehole. Elsewhere it adds some distortion to the centralized images, which can be seen as white (closer) areas around the fallouts. Therefore the truest picture of fallouts is seen on the “Radius”-image and the “Amplitude”-image, as these are not centralized.

### 6.3.2 Example of washout (WO)

In Figure 6-4 an example of washout (WO) from KFM07C is shown. Washouts are separated from breakouts, as there is fallout in the entire perimeter of the borehole, thus the minimum diameter is enlarged. Also here (if possible) a dominating azimuth and aperture angles are read and registered in the Excel sheet.

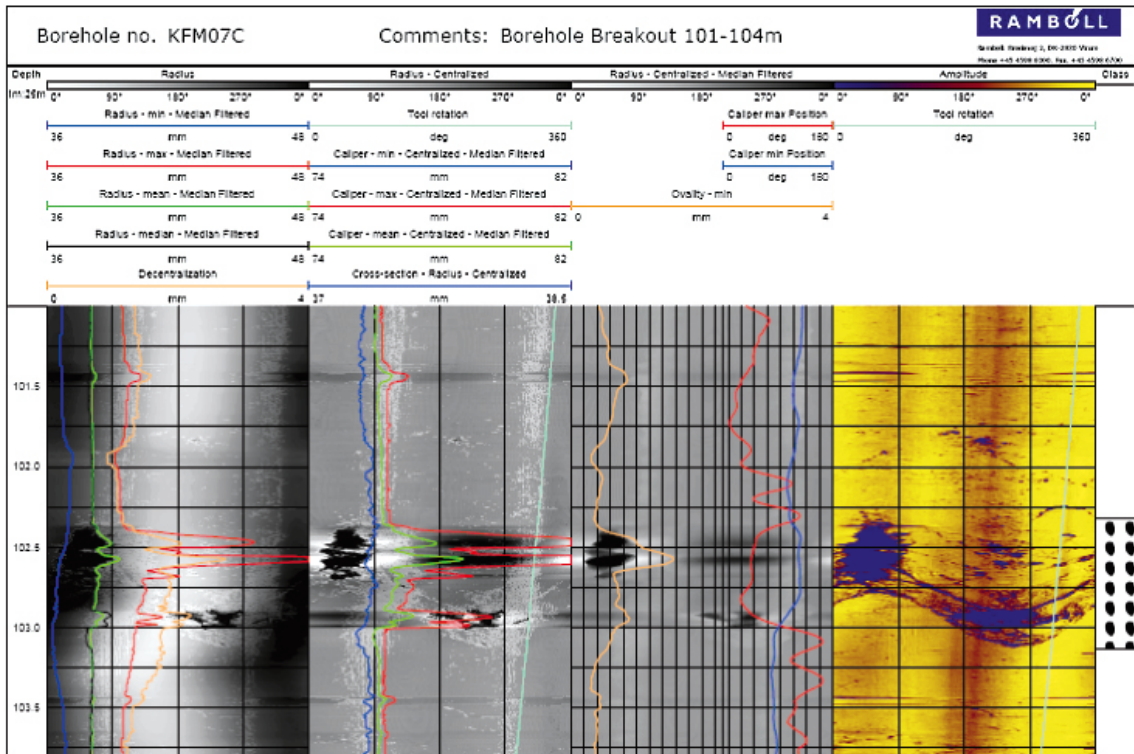


Figure 6-3. Example of borehole breakout from KFM07C.

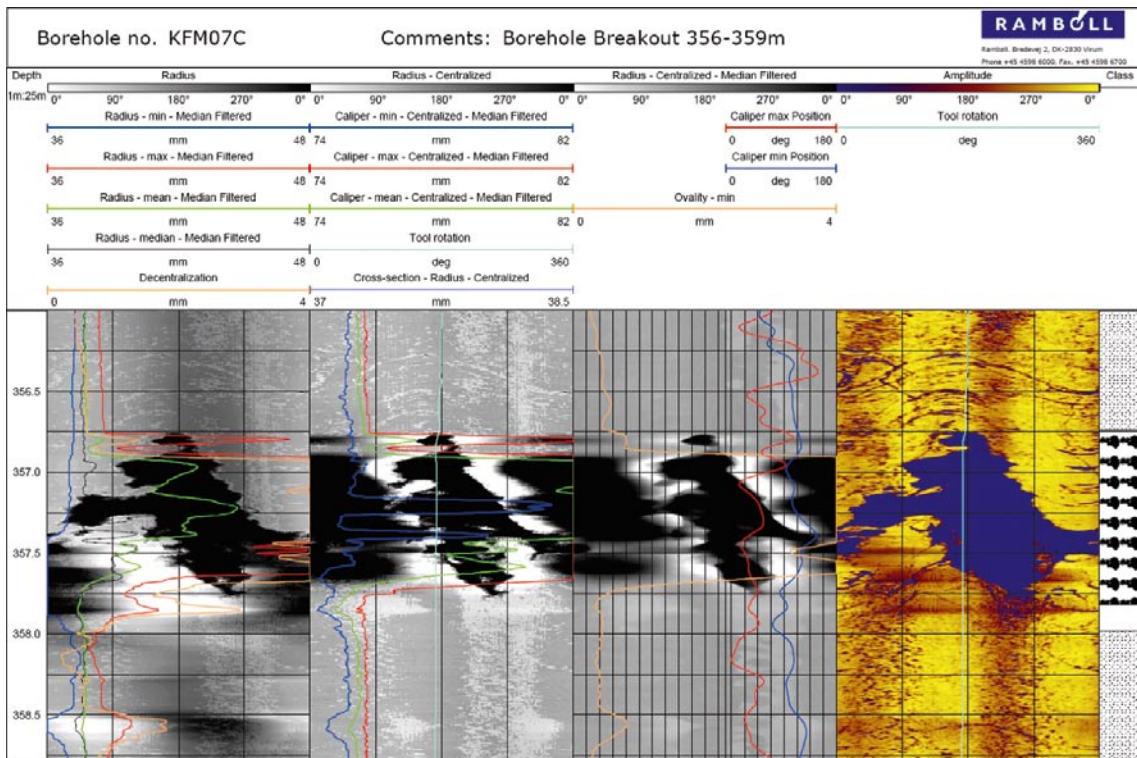


Figure 6-4. Example of washout from KFM07C.



### 6.3.3 Example of keyseat (KS)

In Figure 6-5 an example of a keyseat (KS) from KFM07C is displayed. The keyseat recognised as fallout in only one direction at the relevant depth. Also here azimuth and aperture angles are read and registered in the Excel sheet.

### 6.3.4 Example of micro fallout (MF)

In Figure 6-6 an example of micro fallout is presented. In this example the micro fallout is recognized as two verticals bands in the borehole (which here ends at 205 m). In these cases azimuth and aperture angles are registered. In other cases the fallout is found in the entire circumference of the borehole (with or without a dominating azimuth). In these cases the aperture angles are registered as 0 to 360°.

The micro fallout is mainly recognised on the Amplitude-image. It is sometimes hard to separate from breakouts, but a condition has been set up, that breakouts should be found also on the Radius-images as darker areas – holes. The registration of micro fallout is generally the most uncertain.

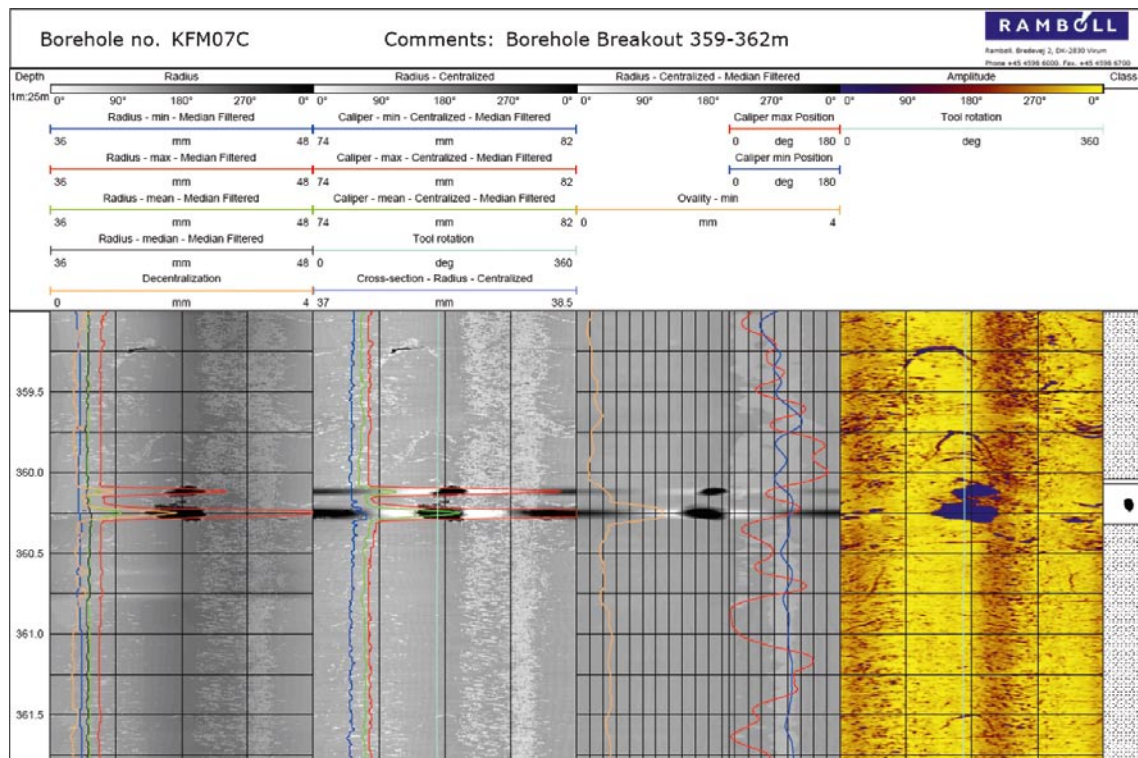


Figure 6-5. Example of keyseat from KFM07C.

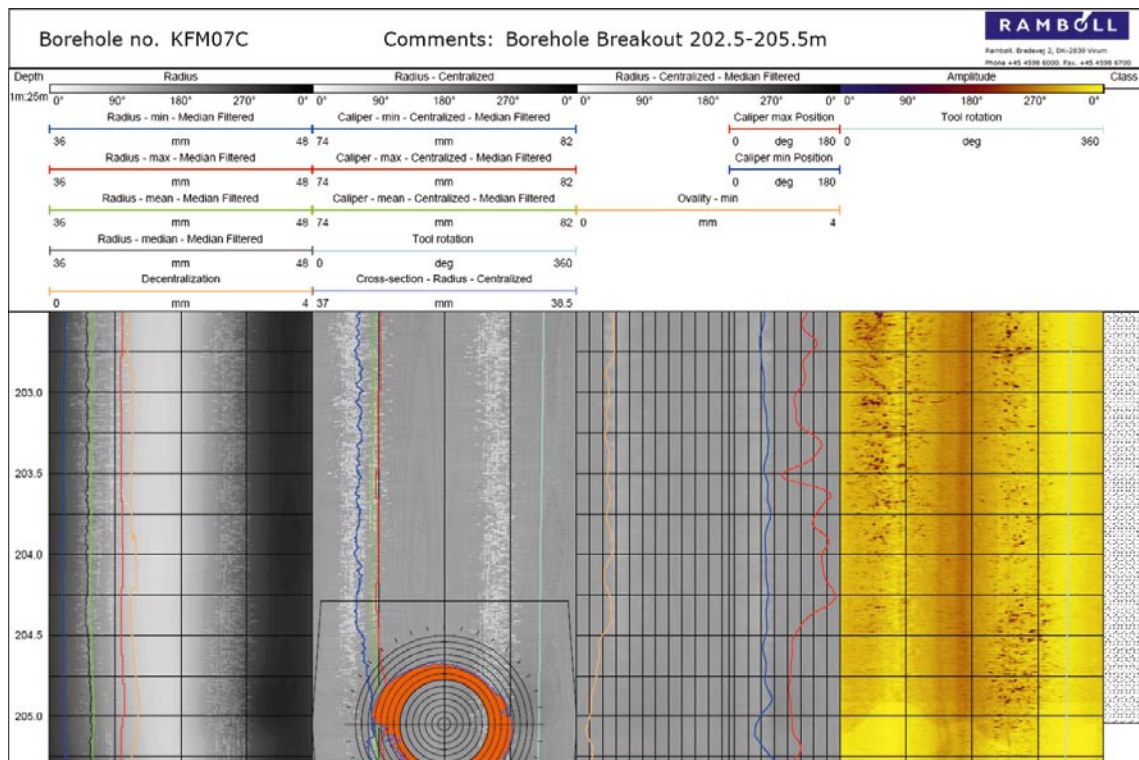


Figure 6-6. Example of micro fallout from KFM07C.

## 6.4 Explanation of special features in the boreholes

### 6.4.1 Tracks from decentralization

In Figure 6-7 a section from KFM01B /Ringgaard 2007/ with different kinds of tracks and shadows found in the boreholes is shown.

- On the Amplitude image dark tracks are seen which follow the rotation of the tool. These tracks have an internal spacing of 90° and come from the centralizers on the acoustic televiewer probe. This is confirmed by the downrun log, on which they not are present.
- The rotation introduces a slight decentralization of the tool, which also follows the rotation. The remedy of the decentralization is explained in the paragraph regarding processing, but it still leaves some darker bands on the images. These darker bands, which follow the tool rotation, are artificial.
- Furthermore some vertical tracks are observed on both the amplitude- and radius-images. They are anticipated to have been made by centralizers from other probes, e.g. the BIPS-probe. In parts of the borehole, they are also recognised on the BIPS-image. /Gustafsson and Gustafsson 2004/.

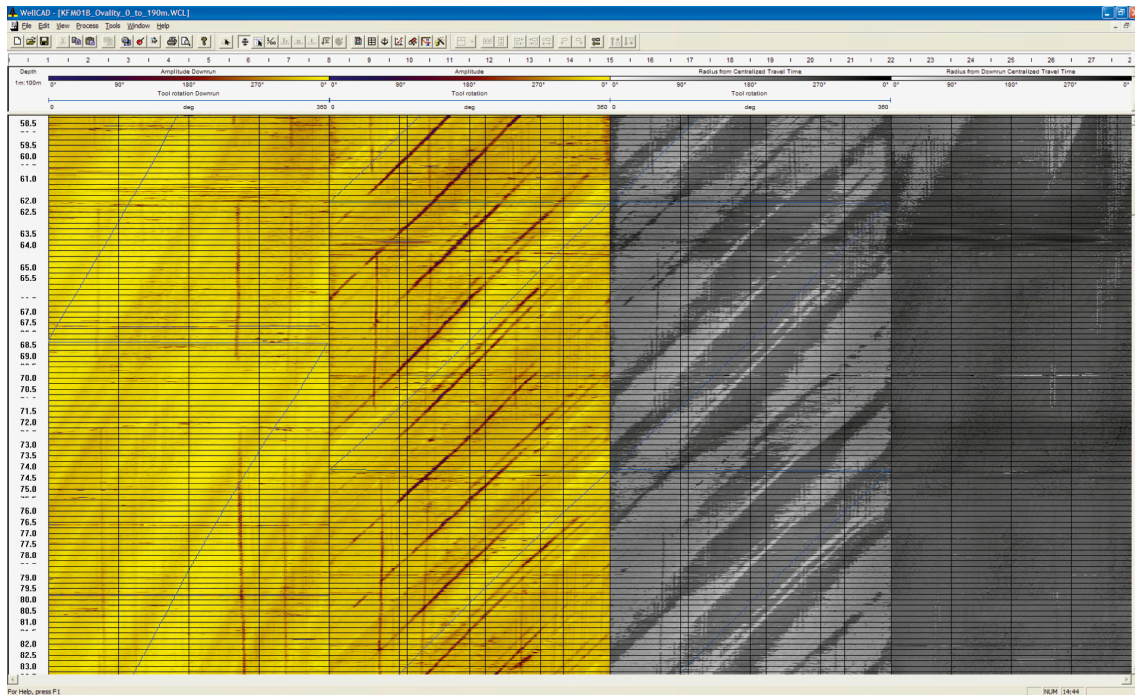


Figure 6-7. Example for tracks and shadows from KFM01B, 58.5 to 83 m.

## 6.4.2 Drill cuttings from bottom of borehole

In Figure 6-8 an example from the bottom of KFM01B is presented. Here drill cuttings from the bottom of the hole have partly covered the acoustic window, but is slowly washed off.

## 6.4.3 Wobbles from drilling process

In Figure 6-9 an example of “wobbles” made by the drilling process is displayed. These wobbles are frequently seen in the boreholes and in some cases they make it hard to register deformations in these areas.

## 6.5 Specific features in the boreholes

### 6.5.1 KFM08A. April 2005

From 100 to 301 metres there is some kind of covering, recognized as blue (low amplitude) areas on the Amplitude image, from 280 to 360° MN.

From 950.0 to 950.4 m there is an error in the datafile.

### 6.5.2 KFM09A

From 48 to 145 metres, there is some covering in a band from 170 to 240° MN.



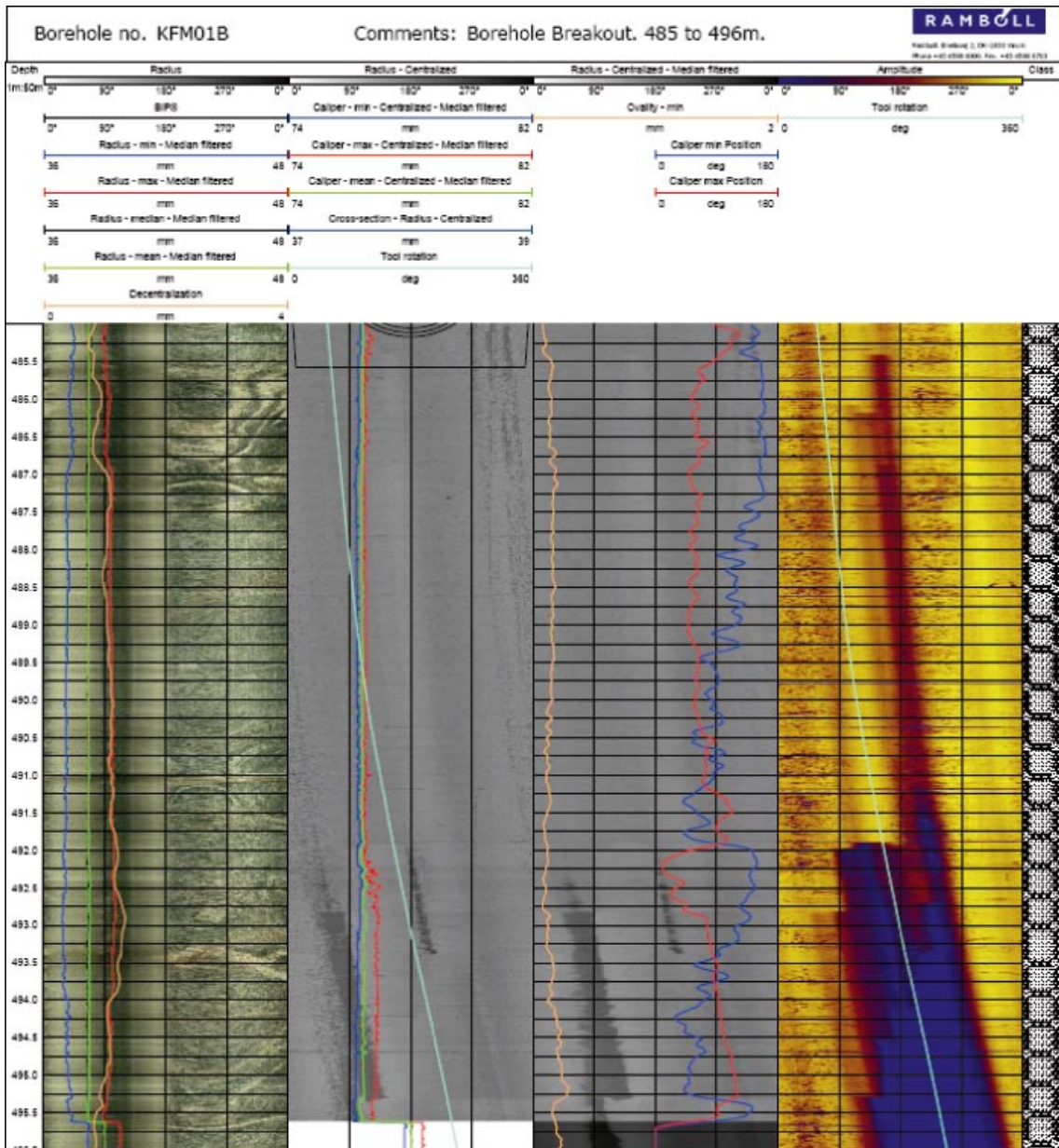


Figure 6-8. Example of drill cuttings on the acoustic window.

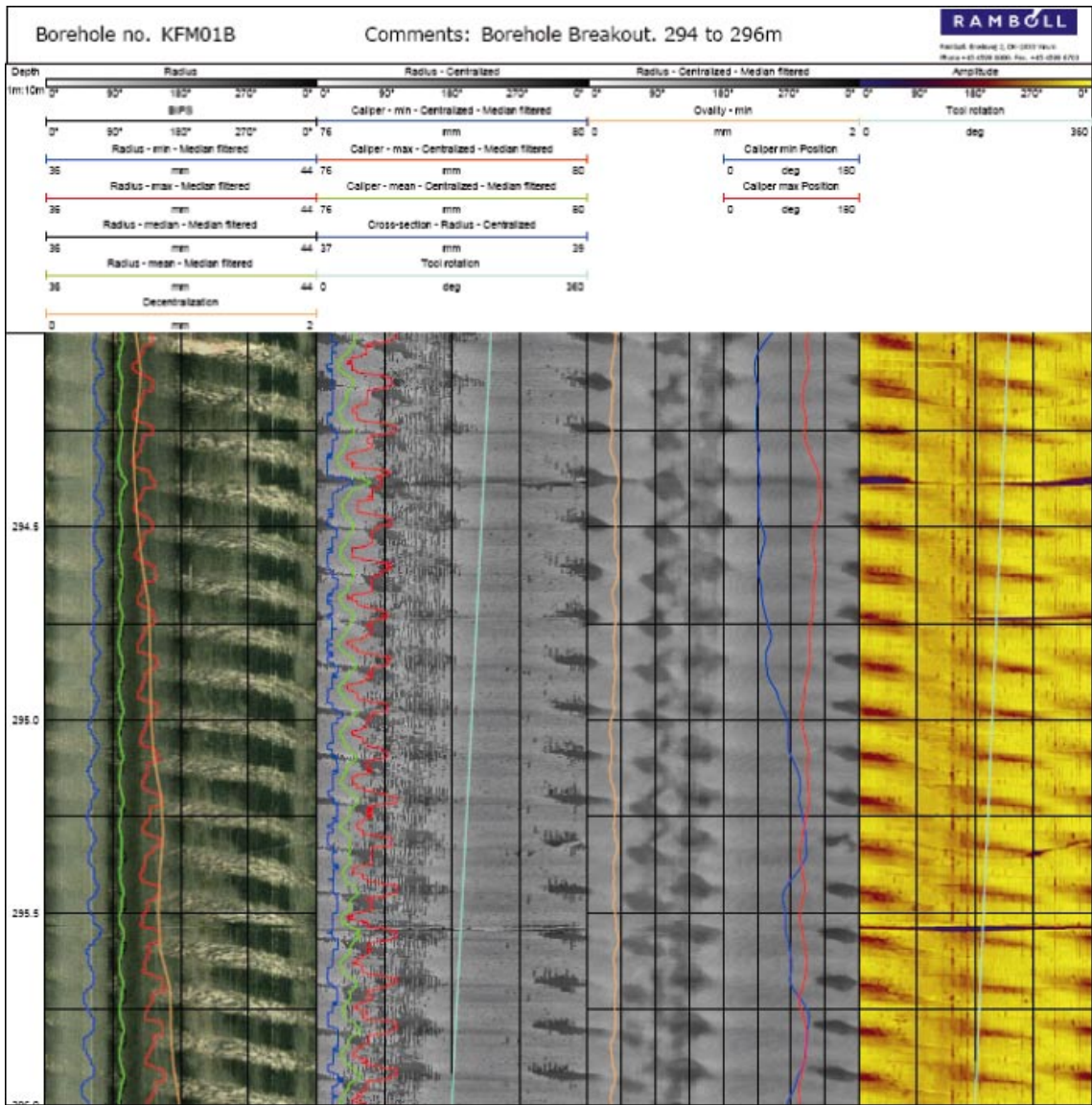


Figure 6-9. Example of wobbles.

## 7 Time dependence of breakout

In an effort to conclude whether breakout caused by the stress field has momentary character, as the drillhole is made or is an ongoing time dependence process, KFM08A has been surveyed twice with the acoustic televiewer. The cored part of KFM08A was drilled from 2005-01-31 to 2005-03-31; the first televiewer survey was performed on 2005-04-28 (4 weeks after the drilling was finished), whereas the second was done in March 2007, i.e. 2 years later.

The deformations registered in KFM08A are shown in Table 7-1.

As seen, the same BB, WO and KS are registered in both surveys. The difference in micro fallout is caused by the different resolution applied in the two surveys. The first survey was made with 2.7×8 mm pixel-size, while the 2007 logging was made with 2×2 mm pixel-size (see also Table 3-1). With the low resolution, the recognition of MF is harder and more unreliable.

The images from the two surveys have been manually inspected side-by-side in a display and there are no signs of any change in the deformations seen.

**Table 7-1. Registered deformations in KFM08A.**

<b>Class</b>	<b>2005</b>	<b>2007</b>
BB	4	4
WO	1	1
KS	1	1
MF	4	17

## 8 Summary and discussions

- It is a relatively quick operation to locate larger deformations, simply by means of scrolling through a calculated high resolution caliper.
- Orientation and size of the deformations can be precisely mapped.
- There is an obvious tendency that the main azimuth of breakouts and micro fallouts in all the boreholes is found to be at 40 to 80° from magnetic north.
- From the study of two surveys in KFM08A with 2 years interval, it is concluded, that no time dependent deformations have taken place in this borehole.
- In boreholes deviated more the 10° from vertical, the cross-sections are often too disturbed of noise from decentralization to be used.
- It is strongly recommended, that the logpanels are evaluated in WellCAD or the free WellCAD-reader, as a print-out or PDF does not provide the necessary flexibility to zoom and focus on relevant deformations.
- When smaller breakouts or micro fallouts are found in connection with fractures, it can be difficult to clarify, whether the fallout was caused by the drilling process or by stress.

## References

- Ask D, Ask M V S, 2006.** Detection of potential borehole breakouts in boreholes KFM01A and KFM01B. SKB P-report in prep., Svensk Kärnbränslehantering AB.
- Ask M V S, Ask D, Christiansson R, 2006.** Detection of borehole breakouts at the Forsmark site, Sweden. Proc. Int. Symp. on in situ Rock Stress (Eds. Lu M, Li CC, Kjörholt H, Dahle H), June 19–21, 2006, Trondheim, Norway, pp. 79–86.
- Deltombe J L, Schepers R, 2000.** Combined Processing of BHTV Traveltime and Amplitude Images. In *Proc. Int. Symp. Borehole Geophysics for Minerals, Geotechnical, and Groundwater applications*, Golden, CO, United States, Vol. 7 pp. 29–42.
- Gustafsson J, Gustafsson C, 2004.** RAMAC- and BIPS-logging in borehole KFM01B and RAMAC directional re-logging in borehole KFM01A. SKB P-04-79, Svensk Kärnbränslehantering AB.
- Plumb R A, Hickman S H, 1985.** Stress-induced borehole elongation: A comparison between four-arm dipmeter and the borehole televiewer in the Auburn geothermal well. *J. Geophys. Res.*, 90, p. 5513–21.
- Ringgaard, 2007.** Mapping of borehole breakouts. Processing of acoustical televiewer data from KFM01A, KFM01B, KFM02A, KFM03A, KFM03B, KFM04A, KFM05A, KFM06A and KFM07C. SKB P-07-07, Svensk Kärnbränslehantering AB.
- Siddans A W B, Worthington P, 2003.** Structural geology using borehole wall imagery. Case studies of 3 HiRAT logs. Not published, can be found on Robertson Geologgings homepage.
- Zoback M D, Moos D, Martin L, Andersson R N, 1985.** Borehole breakouts and in situ stress. *J. Geophys. Res.*, 90, pp. 5523–30.

# Appendices on CD

**Appendix A** List of acquisition reports

**Appendix B** Tables and charts of depth errors

**KFM08A**

**KFM08C**

**KFM09A**

**KFM09B**

**Appendix C** Tables and charts of registered deformations

**KFM08A. April 2005**

**KFM08A. March 2007**

**KFM08C**

**KFM09A**

**KFM09B**

**KFM90B**

**Appendix D** Plot of logpanels

**Appendix D KFM08A\_Breakout\_April\_2005**

**Appendix D KFM08A\_Breakout\_March\_2007**

**Appendix D KFM08C\_Breakout**

**Appendix D KFM09A\_Breakout**

**Appendix D KFM09B\_Breakout**

**Appendix D KFM90B\_Breakout**



### List of acquisition reports

List of acquisition reports from logging with acoustic televiewer, fluid temperature and resistivity – and calculation of fluid velocity.

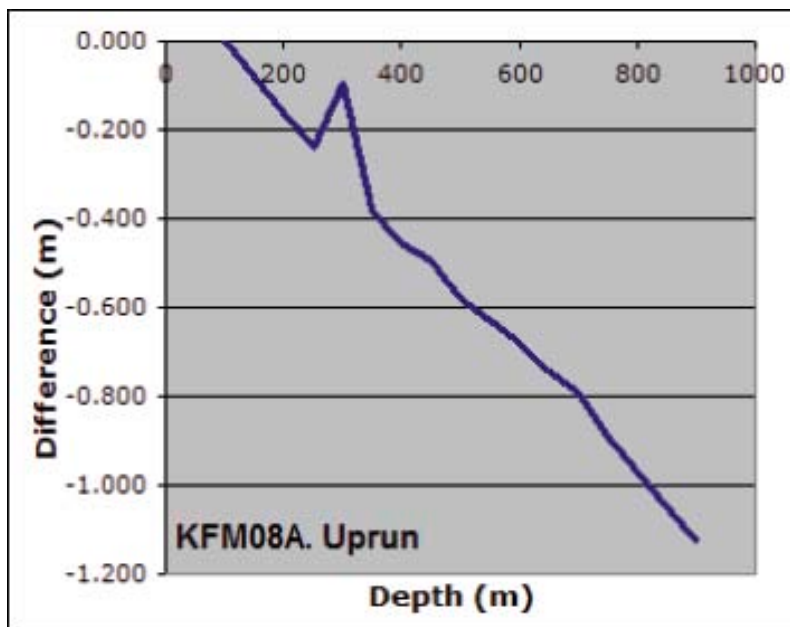
- KFM08A: SKB P-05-159. Geophysical borehole logging in the boreholes KFM07A, KFM08A and KFM08B. Forsmark site investigation. Nielsen, Uffe Torben; Ringgaard, Jørgen; Fris Dahl, Jesper. 2005.
- KFM08C: SKB P-07-05. Geophysical borehole logging in boreholes KFM08C, KFM10A, HFM30, HFM31, HFM33, HFM34, HFM35 and HFM38. Forsmark site investigation. Nielsen, Uffe Torben; Ringgaard, Jørgen. 2007.
- KFM09A: SKB P-06-22. Geophysical borehole logging in boreholes KFM09A, KFM07B, HFM25, HFM27 and HFM28. Forsmark site investigation. Nielsen, Uffe Torben; Ringgaard, Jørgen; Vangkilde-Pedersen, Thomas. 2006.
- KFM09B: SKB P-06-123. Geophysical borehole logging in boreholes KFM01C, KFM09B, HFM07, HFM24, HFM26, HFM29 and HFM32. Forsmark site investigation. Nielsen, Uffe Torben; Ringgaard, Jørgen; Fris Dahl, Jesper. 2006.
- KFM90B: SKB P-07-092. Geophysical borehole logging in boreholes KFM11A and KFM90B. Forsmark site investigation. Nielsen, Uffe Torben; Ringgaard, Jørgen. 2007.

Tables and charts of depth errors

**KFM08A**

**KFM08A. April 2005. Uprun**

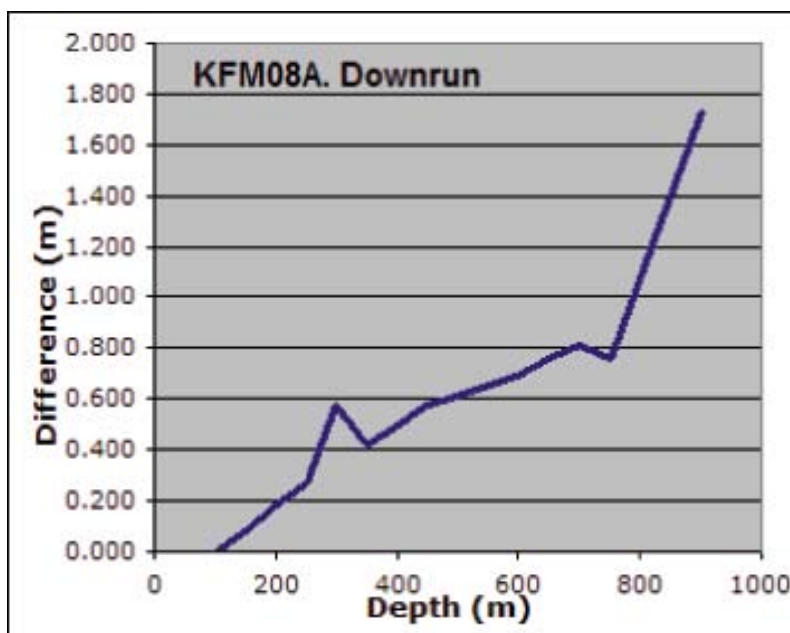
True depth [m]	HiRAT [m]	Difference [m]
102.260	102.260	0.000
151.000	151.080	-0.080
200.000	200.158	-0.158
250.000	250.239	-0.239
300.000	300.097	-0.097
350.000	350.380	-0.380
400.000	400.456	-0.456
450.000	450.496	-0.496
500.000	500.581	-0.581
600.000	600.679	-0.679
650.000	650.743	-0.743
700.000	700.788	-0.788
750.000	750.896	-0.896
900.000	901.125	-1.125



Not used tracks at 300 m for stretch

**KFM08A. April 2005. Downrun**

True depth [m]	HiRAT [m]	Difference [m]
102.260	102.260	0.000
151.000	150.925	0.075
200.000	199.820	0.180
250.000	249.727	0.273
300.000	299.420	0.580
350.000	349.580	0.420
400.000	399.500	0.500
450.000	449.420	0.580
500.000	499.390	0.610
600.000	599.310	0.690
650.000	649.240	0.760
700.000	699.190	0.810
750.000	749.240	0.760
900.000	898.270	1.730



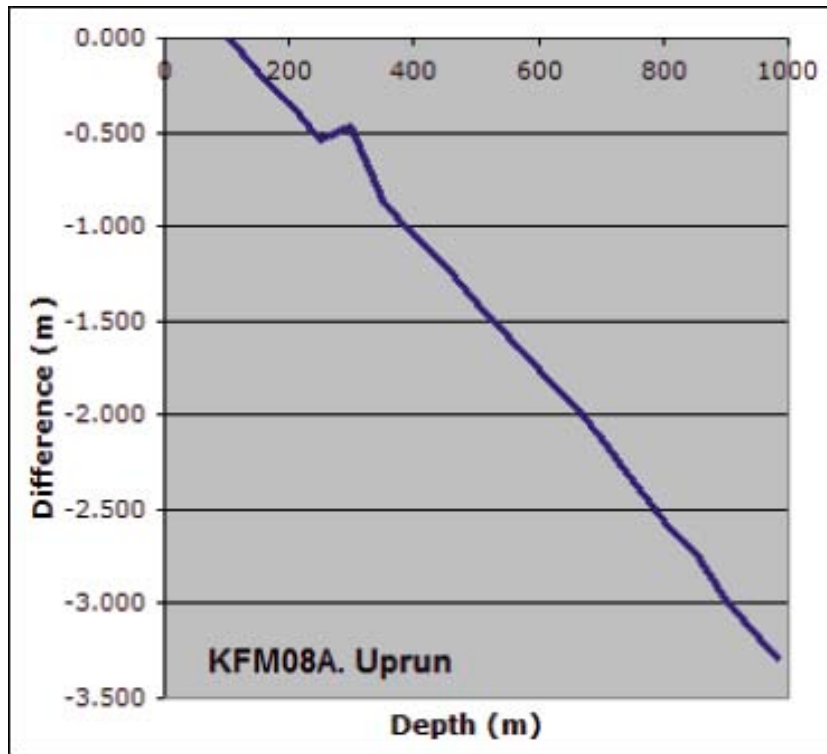
Not used tracks at 300 m for stretch



**KFM08A. March 2007. Uprun**

True depth [m]	HiRAT [m]	Difference [m]
102.260	102.260	0.000
151.000	151.180	-0.180
200.000	200.346	-0.346
250.000	250.538	-0.538
300.000	300.470	-0.470
350.000	350.860	-0.860
400.000	401.046	-1.046
450.000	451.194	-1.194
500.000	501.407	-1.407
600.000	601.761	-1.761
650.000	651.932	-1.932
700.000	702.128	-2.128
750.000	752.346	-2.346
800.000	802.556	-2.556
850.000	852.728	-2.728
900.000	902.982	-2.982
981.000	984.291	-3.291

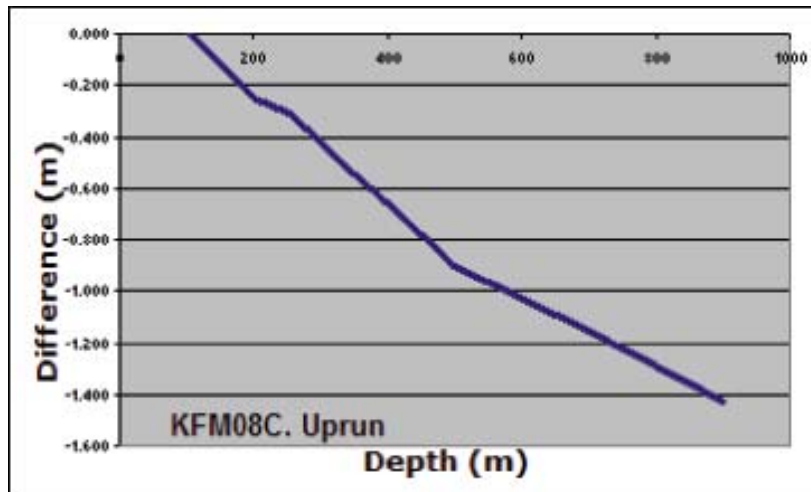
Not used tracks at 300 m for stretch



**KFM08C**

**KFM08C. Uprun**

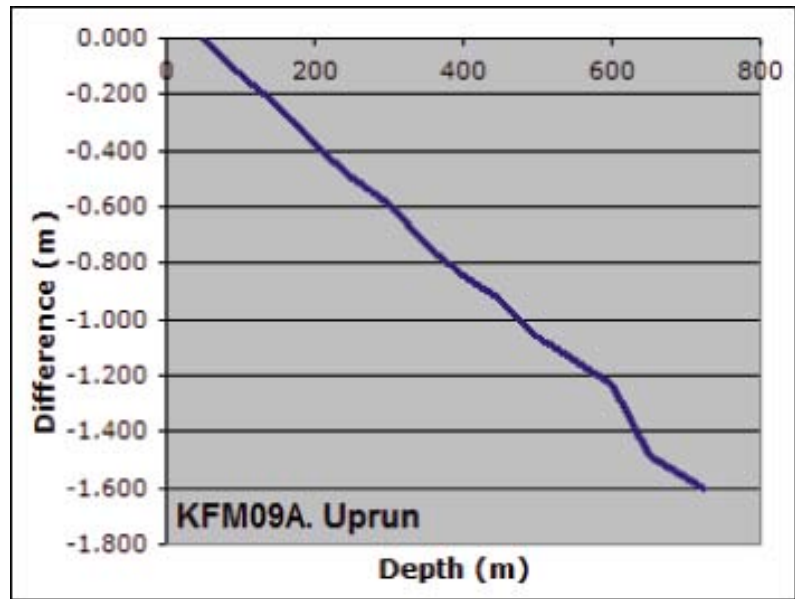
True depth [m]	HiRAT [m]	Difference [m]
102.230	102.230	0.000
150.000	150.114	-0.114
200.000	200.250	-0.250
250.000	250.310	-0.310
300.000	300.423	-0.423
350.000	350.551	-0.551
398.000	398.652	-0.652
450.000	450.787	-0.787
500.000	500.899	-0.899
700.000	701.150	-1.150
900.000	901.430	-1.430



## KFM09A

### KFM09A. Uprun

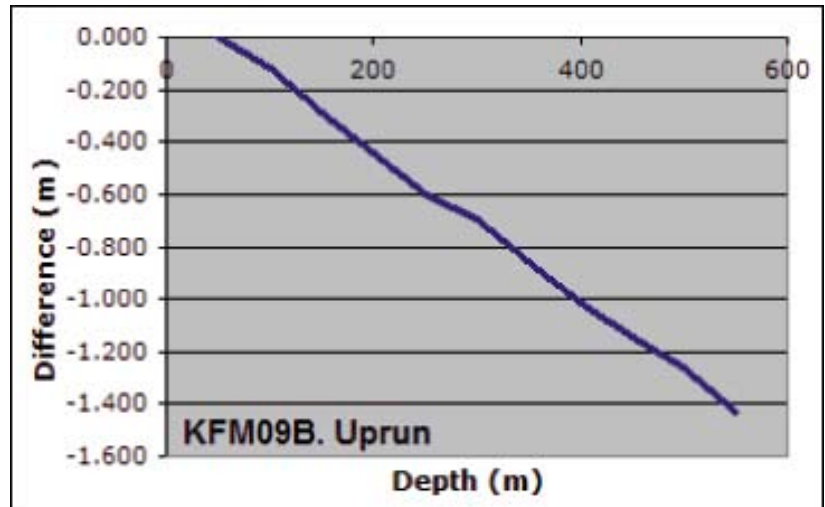
True depth [m]	HiRAT [m]	Difference [m]
50.000	50.000	0.000
99.000	99.127	-0.127
150.000	150.239	-0.239
200.000	200.380	-0.380
250.000	250.498	-0.498
300.000	300.594	-0.594
350.000	350.737	-0.737
400.000	400.841	-0.841
450.000	450.930	-0.930
500.000	501.069	-1.069
550.000	551.146	-1.146
600.000	601.234	-1.234
650.000	651.486	-1.486
725.000	726.602	-1.602



## KFM09B

### KFM09B. Uprun

True depth [m]	HiRAT [m]	Difference [m]
50.000	50.000	0.000
100.000	100.117	-0.117
150.000	150.285	-0.285
200.000	200.440	-0.440
250.000	250.605	-0.605
300.000	300.693	-0.693
350.000	350.857	-0.857
400.000	401.017	-1.017
450.000	451.141	-1.141
500.000	501.258	-1.258
550.000	551.428	-1.428

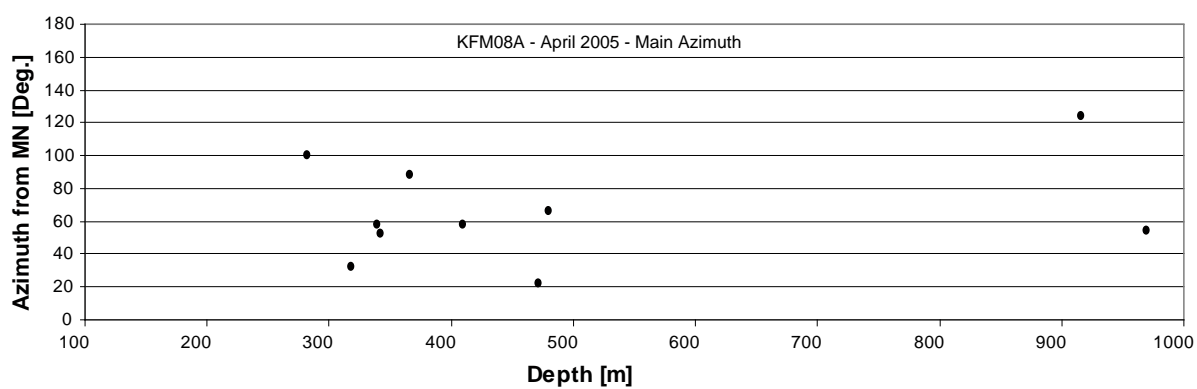


## Tables and charts of registered deformations

### KFM08A. April 2005

#### KFM08A April 2005 – Observed BB, WO, MF and KS

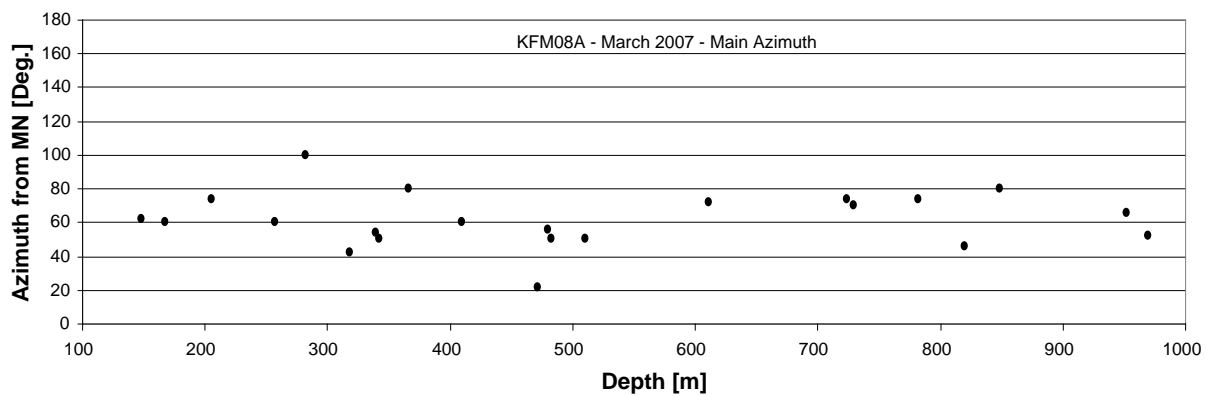
Top Depth [m]	Bot. depth [m]	Max R [mm]	Median R [mm]	dRmax [mm]	Class	Uncertainty [0-3]	Cross. struct. [Yes/No]	Main Azimuth [Deg. from MN]	Azimuth [Deg. from MN]	Aperture $\alpha$ 1 [Deg. from MN]	Aperture $\alpha$ 2 [Deg. from MN]	Comments
281.70	281.93	46.0	38.0	8.0	BB	3	Y	100	280	222	322	
317.97	318.10	43.0	38.1	4.9	KS	3	N	32	32	0	58	
339.57	340.25	38.3	38.0	0.3	MF	1	Y	58	58	0	95	
342.00	343.24	38.2	38.0	0.2	MF	1	Y	52	232	136	306	
365.85	366.24	50.0	37.9	12.1	BB	3	Y	88	268	204	325	
409.91	412.12	38.3	38.0	0.3	MF	2	N	58	58	0	360	
471.01	471.31	38.2	38.0	0.2	MF	1	N	22	22	-10	75	
480.13	482.06	50.0	38.1	11.9	BB	1	Y	66	66	0	180	
915.75	920.50	115.0	38.4	76.6	WO	1	Y	124	304	0	360	
969.34	969.58	40.8	39.0	1.8	BB	2	N	54	234	192	276	



# KFM08A. March 2007

## KFM08A March 2007 – Observed BB, WO, MF and KS

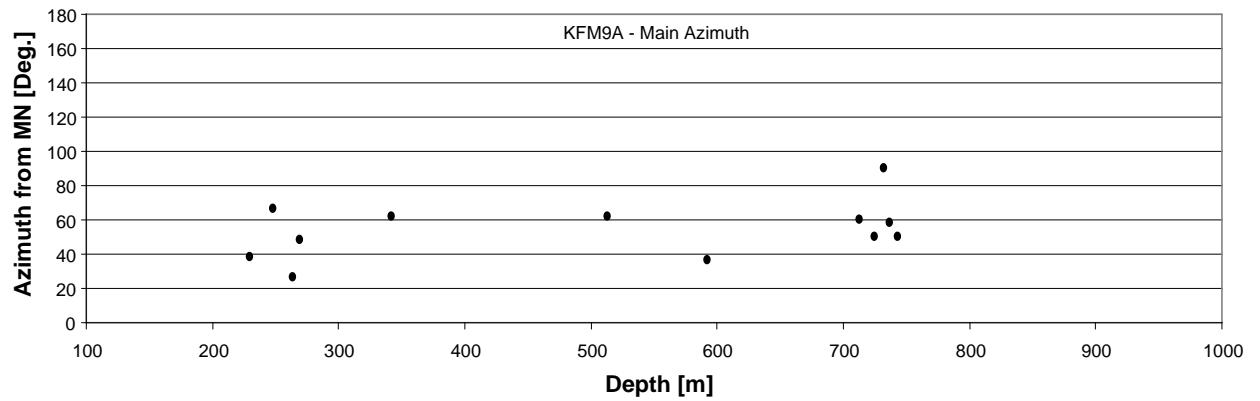
Top Depth [m]	Bot. depth [m]	Max R [mm]	Median R [mm]	dRmax [mm]	Class	Uncertainty [0-3]	Cross. struct. [Yes/No]	Main Azimuth [Deg. from MN]	Azimuth [Deg. from MN]	Aperture $\alpha$ 1 [Deg. from MN]	Aperture $\alpha$ 2 [Deg. from MN]	Comments
147.71	153.31	38.6	38.5	0.1	MF	1	N	62	62	20	90	
167.60	170.36	38.6	38.5	0.1	MF	1	N	60	60	20	90	
205.00	246.90	38.6	38.5	0.1	MF	1	N	74	74	44	95	
257.50	262.37	38.7	38.6	0.1	MF	1	N	60	60	30	95	
281.66	281.93	45.0	38.3	6.7	BB	3	Y	100	280	222	322	
317.82	318.13	44.4	38.4	6.0	KS	3	N	42	42	12	70	
339.57	340.35	38.4	38.3	0.1	MF	2	Y	54	54	0	360	
342.00	343.24	38.4	38.3	0.1	MF	2	Y	50	230	136	328	
365.85	366.24	49.0	38.4	10.6	BB	3	Y	80	260	204	328	
409.88	412.12	38.5	38.4	0.1	MF	2	Y	60	60	0	360	
471.01	471.31	38.5	38.4	0.1	MF	1	N	22	22	-10	75	
480.13	482.06	52.0	38.3	13.7	BB	2	Y	56	56	0	180	
482.15	493.50	38.4	38.3	0.1	MF	2	N	50	50	10	100	
510.00	519.00	38.4	38.3	0.1	MF	1	N	50	50	20	102	
610.75	630.00	38.4	38.3	0.1	MF	1	N	72	72	0	100	
724.00	728.00	38.4	38.3	0.1	MF	2	N	74	74	0	360	
729.30	731.10	39.5	39.0	0.5	MF	1	N	70	70	0	360	
782.00	795.00	38.4	38.3	0.1	MF	1	N	74	74	0	360	
820.18	821.52	38.3	38.2	0.1	MF	2	N	46	46	0	360	
848.60	852.10	38.5	38.4	0.1	MF	2	N	80	80	0	360	
915.75	920.50	115.0	38.5	76.5	WO	1	Y			0	360	
951.50	966.00	38.7	38.6	0.1	MF	1	N	66	66	0	360	
969.34	969.58	43.0	38.6	4.4	BB	2	N	52	232	182	272	



# KFM08C

## KFM08C – Observed BB, WO, MF and KS

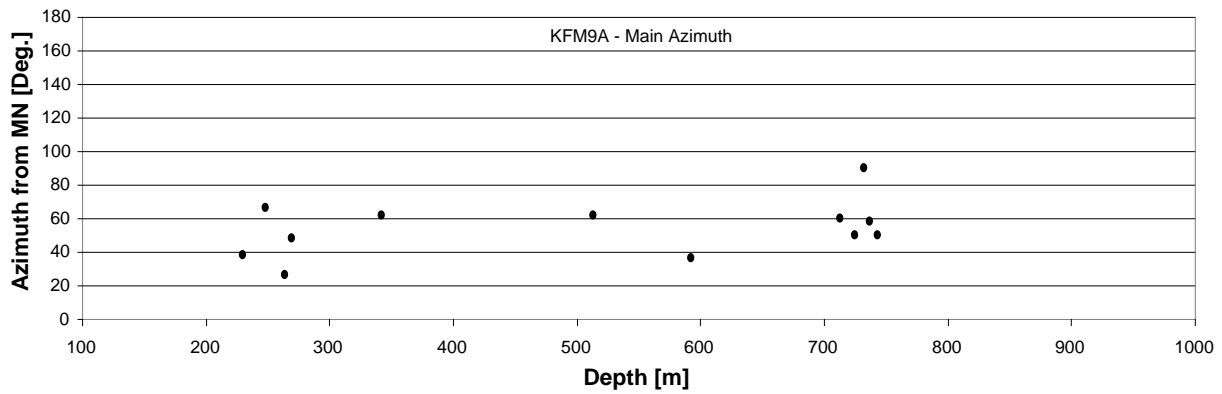
Top Depth [m]	Bot. depth [m]	Max R [mm]	Median R [mm]	dRmax [mm]	Class	Uncertainty [0-3]	Cross. struct. [Yes/No]	Main Azimuth [Deg. from MN]	Azimuth [Deg. from MN]	Aperture $\alpha_1$ [Deg. from MN]	Aperture $\alpha_2$ [Deg. from MN]	Comments
180.60	182.27	41.0	38.4	2.6	BB	2	Y	52	52	32	72	
244.36	245.88	39.0	38.8	0.2	MF	2	Y			0	360	
454.77	458.36	38.8	38.6	0.2	MF	3	N	124	124	0	360	
456.00	459.56	39.2	38.6	0.6	BB	2	Y	136	136	90	180	
479.62	479.75	102.0	38.4	63.6	KS	3	N	34	34	-5	80	
497.84	499.03	102.0	38.5	63.5	BB	3	N	102	102	0	180	
519.17	521.17	38.4	38.3	0.1	MF	2	N			0	360	
522.75	525.81	38.6	38.5	0.1	MF	3	N	129	309	0	360	
529.71	532.06	38.7	38.6	0.1	MF	3	N	130	130	80	350	
533.33	533.85	38.7	38.6	0.1	MF	2	N	122	122	80	320	
624.50	628.20	38.3	38.2	0.1	MF	1	N	124	124	66	160	
692.57	695.80	47.0	38.7	8.3	BB	3	N	24	24	-10	50	
726.72	727.89	40.0	38.6	1.4	MF	3	N	52	52	0	250	
756.30	752.08	38.6	38.5	0.1	MF	1	N	69	69	0	180	
829.55	831.17	45.0	38.6	6.4	BB	3	Y	56	56	-20	90	
831.20	834.10	38.7	38.6	0.1	MF	2	N	56	56	0	90	
878.00	882.30	38.7	38.6	0.1	MF	1	N			0	360	



# KFM09A

## KFM09A – Observed BB, WO, MF and KS

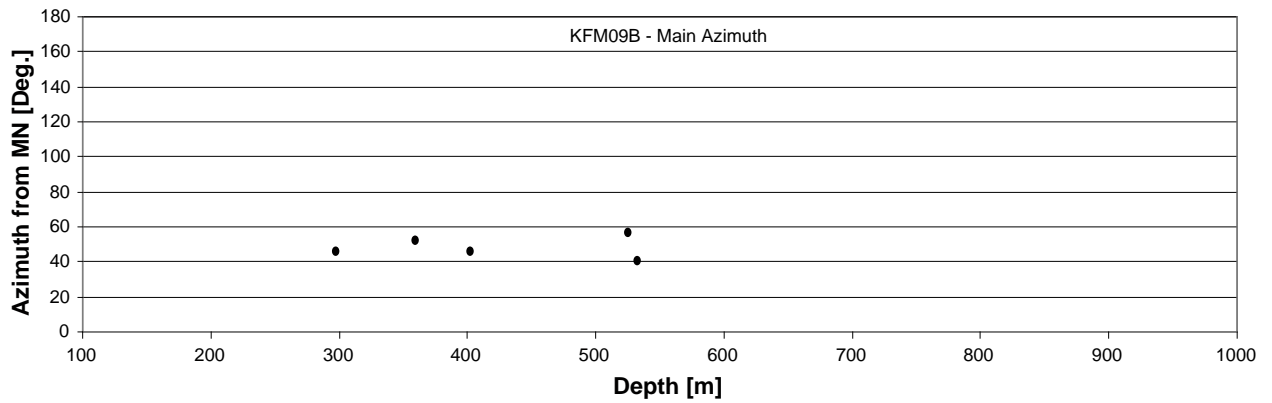
Top Depth [m]	Bot. depth [m]	Max R [mm]	Median R [mm]	dRmax [mm]	Class	Uncertainty [0-3]	Cross. struct. [Yes/No]	Main Azimuth [Deg. from MN]	Azimuth [Deg. from MN]	Aperture $\alpha 1$ [Deg. from MN]	Aperture $\alpha 2$ [Deg. from MN]	Comments
13.00	17.25	39.5	39.3	0.2	BB	2	N	74	74	5	90	
68.93	77.76	40.0	38.9	1.1	MF	3	N	83	83	20	330	
230.08	232.81	50.0	38.3	11.7	BB	3	N	38	218	188	258	
233.00	247.50	38.4	38.3	0.1	MF	1	N			0	360	
247.75	252.78	40.8	38.3	2.5	BB	3	Y	66	66	28	114	
263.60	269.15	46.0	38.2	7.8	BB	3	N	26	26	-40	90	
269.30	282.30	38.2	38.1	0.1	MF	2	N	48	48	0	360	
341.59	351.12	39.1	38.1	1.0	MF	3	N	62	62	24	102	
513.58	520.05	38.2	38.1	0.1	MF	3	N	62	62	0	360	
591.88	592.00	43.0	38.0	5.0	BB	3	N	36	36	0	95	
699.25	705.13	38.2	38.1	0.1	MF	2	N			0	360	
713.17	717.90	38.3	38.2	0.1	MF	1	N	60	240	0	360	
725.00	732.00	38.6	38.1	0.5	MF	3	N	50	230	0	360	
732.00	734.70	50.0	38.2	11.8	WO	3	N	90	90	0	360	
737.19	739.61	55.0	38.2	16.8	BB	2	Y	58	58	0	100	
743.37	746.20	46.0	38.2	7.8	WO	1	Y	50	50	0	360	



## KFM09B

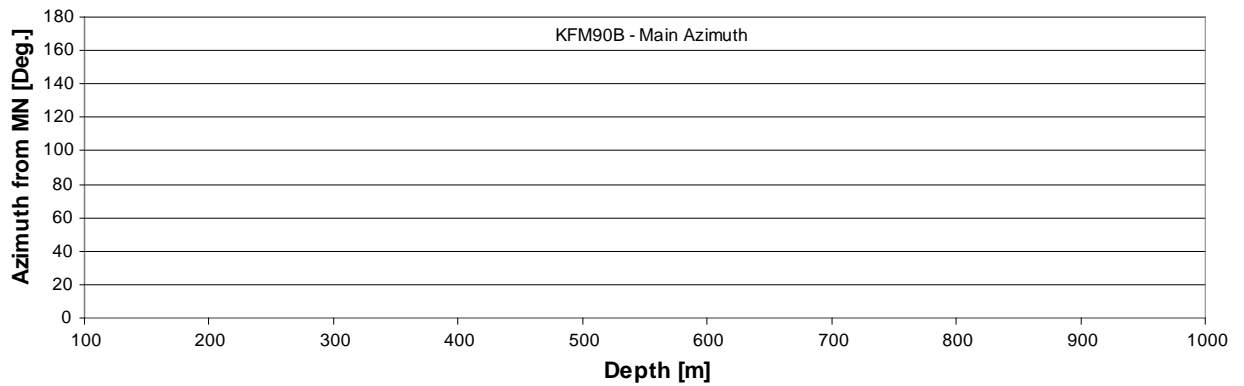
### KFM09B – Observed BB, WO, MF and KS

Top Depth [m]	Bot. depth [m]	Max R [mm]	Median R [mm]	dRmax [mm]	Class	Uncertainty [0-3]	Cross. struct. [Yes/No]	Main Azimuth [Deg. from MN]	Azimuth [Deg. from MN]	Aperture $\alpha 1$ [Deg. from MN]	Aperture $\alpha 2$ [Deg. from MN]	Comments
16.47	20.36	40.8	38.8	2.0	WO	1	Y	58	58	0	360	
27.20	34.20	38.9	38.3	0.6	MF	2	N	74	74	0	360	
90.84	95.89	38.2	38.1	0.1	MF	2	N	62	242	180	270	
114.30	121.90	38.1	38.0	0.1	MF	1	N			0	360	
139.00	174.80	38.4	38.3	0.1	MF	1	N			0	360	
297.43	297.97	39.5	37.9	1.6	BB	3	N	46	46	-5	90	
359.30	360.13	38.2	38.1	0.1	MF	3	N	52	232	200	270	
402.10	402.50	42.0	38.0	4.0	BB	1	Y	46	226	185	285	
525.16	529.90	56.0	38.2	17.8	BB	3	N	56	56	-15	145	
532.67	532.79	42.4	38.0	4.4	BB	3	Y	40	40	0	90	
567.80	573.30	41.0	38.0	3.0	MF	3	N			0	360	Includes some larger fallouts



## KFM90B

Top Depth [m]	Bot. depth [m]	Max R [mm]	Median R [mm]	dRmax [mm]	Class	Uncertainty [0-3]	Cross. struct. [Yes/No]	Main Azimuth [Deg. from MN]	Azimuth [Deg. from MN]	Aperture $\alpha 1$ [Deg. from MN]	Aperture $\alpha 2$ [Deg. from MN]	Comments
				0.0					0			



**Plot of logpanels**

**KFM08A\_Breakout\_April\_2005.pdf**

**KFM08A\_Breakout\_March\_2007.pdf**

**KFM08C\_Breakout.pdf**

**KFM09A\_Breakout.pdf**

**KFM09B\_Breakout.pdf**

**KFM90B\_Breakout.pdf**